J Mol Model (2014) 20:2375
DOI 10.1007/s00894-014-2375-5

ORIGINAL PAPER

Europium doped zinc sulfide: a correlation between experimental and theoretical calculations

Mateus M. Ferrer · Yuri V. B. de Santana · Cristiane W. Raubach · Felipe A. La Porta · Amanda F. Gouveia · Elson Longo · Julio R. Sambrano

Received: 12 March 2014 / Accepted: 30 June 2014 / Published online: 1 August 2014

Abstract
This paper presents the correlation among electronic and optical property effects induced by the addition of different concentrations of europium (Eu^{3+}) in zinc sulfide (ZnS) by microwave-assisted solvothermal (MAS) method. A shift of the photoluminescence (PL) emission was observed with the increase of Eu^{3+}. The periodic DFT calculations with the B3LYP hybrid functional were performed using the CRYSTAL computer code. The UV–vis spectra and theoretical results indicate a decrease in behavior of the energy gap as a function of dopant concentration. Therefore, new localized states are generated in the forbidden band gap region, the new states increase the probability of less energy transitions which may be responsible for a red shift in the PL bands spectrum.

Keywords B3LYP · DFT · Doping process · Eu · Microwave · Photoluminescence · ZnS

This paper belongs to Topical Collection QUITEL 2013

M. M. Ferrer · Y. V. B. de Santana · C. W. Raubach · A. F. Gouveia
INCTMN-UFSCar, Universidade Federal de São Carlos, P.O. Box 676, 13565-905 São Carlos, SP, Brazil

F. A. La Porta · E. Longo
INCTMN-UNESP, São Paulo State University, P.O. Box 355, 14801-907 Araraquara, SP, Brazil

J. R. Sambrano (✉)
Grupo de Modelagem e Simulação Molecular, INCTMN-UNESP, São Paulo State University, P.O. Box 473, 17033-360 Bauru, SP, Brazil
e-mail: sambrano@fc.unesp.br

Introduction

Luminescent materials such as rare earth doped powders have attracted attention due to their possible photonic applications [1–4]. Among several rare earths reported, trivalent europium (Eu^{3+}), which has been recognized as efficient luminophore, is one of the most studied, mainly due to non-degenerated levels involved in electronic transitions [5–8]. Emission spectra of the Eu^{3+} ion show narrow sharp bands due to 4f-4f intraconfiguration transitions protection by external $5s^2$ and $5p^6$ sub-shells [9]. For this reason, the Eu^{3+} ion is used as luminescent probe because it is little affected by chemical environment changes; this characteristic may be important to improve the development of materials science.

Furthermore, the doping process in semiconductors produces changes in structural and electronic properties of materials, which is an efficient way to further enhance their properties and applications [10]. A suitable host must also possess a large optical band gap as well as good solubility and stability. In particular, zinc sulfide (ZnS) is suitable as a host matrix. It is an important II-VI semiconductor material with a wide band gap (about 3.72 eV for the cubic zinc blende phase, and 3.77 eV for the wurtzite phase in bulk materials at 300 K) [11–13]. By doping with different metal ions (including transition metals and rare earths), it is possible to realize full-color luminescence in the UV–visible region [14]. Thus, a number of publications concerning well-formed ZnS nanocrystals doped with various types of impurities have appeared in recent years [15–18]. In addition, impurities can produce drastic changes in optical behaviors. These effects can be used as an important tools in lighting and display areas.

Eu^{3+} as a dopant in ZnS has been prepared by chemical vapor deposition (1073 K and 10 min), solid-state reaction (1573 K and 60 min), sol–gel, solvothermal (413 K and 300 min) and other synthetic methods [15–17, 19]. Therefore, it is important to develop new low cost and

environmentally friendly processing material methods with the possibility of the formation of materials at the micro and nanoscale level with well-defined morphologies. Recently, the microwave-assisted solvothermal (MAS) method has emerged as an alternative in field of powder preparation with both expected and unexpected merits; e.g., kinetic enhancement, low reaction temperature and time reduction as well as the control of the overall particle size and aggregation process [20, 21]. The ability to achieve a high temperature stable phase at very low temperatures not only provides an economically viable route for applications, but also opens a new way to study the structural kinetics and chemistry of nanocrystals and various functional materials [22–24]. Very recently, our group conducted experimental studies of ZnS and CdS obtained with MAH method and showed its ease and efficiency enabling a range of studies that can be done. In the case of ZnS, it was possible to obtain the organized phase in 413 K and 1 min [23–26].

Changes induced by addition of different concentrations of Eu^{3+} (1, 2 and 4 %) in the pure ZnS prepared by the MAS method are reported. A systematic investigation of the structural, electronic, and optical properties of doped ZnS zinc-blend (cubic) structure as a function of different concentrations of Eu^{3+}. In order to explain experimental outcomes, quantum mechanical results were calculated based on the density functional theory (DFT) at the B3LYP level. Changes caused in optical properties illustrate the kinds of defects which are caused by europium addition.

Methods

Sample preparation

To obtain pure ZnS, anhydrous $ZnCl_2$ (3.67 mmols) was dissolved in 25 mL of ethylene glycol. Subsequently, 4.74 mmols of tetramethylammonium hydroxide (TMAH) in a methanol solution was added (solution 1). Separately, 3.67 mmol of thiourea was dissolved in 25 mL of ethylene glycol (solution 2). Under stirring, solution 2 was quickly added into solution 1. The resulting solution was transferred to a reactor coated with polytetrafluoroethylene (PTFE) and placed into a domestic Microwave-Solvothermal (MS) system (2.45 GHz, maximum power of 800 W). The MAS processing was performed at 413 K for 16 min. The resulting solution was washed with deionized water and ethanol several times to neutralize the solution pH (≈7) and the precipitates were finally collected and dried at 343 K for 24 h.

Different concentrations of $EuCl_3$ were dissolved in solution 1 according to the desired dopant concentration (1, 2 and 4 % nominal) to obtain the ZnS doped with Eu^{3+} (ZnS:Eu).

Characterization techniques

The obtained powders were characterized by X-ray diffraction (XRD) (Rigaku DMax 2500PC using Cu $K_{\alpha1}$ (λ=1.5406 Å) and Cu $K_{\alpha2}$ (λ=1. 54434 Å) radiation setup) and field emission scanning electron microscopy (FE-SEM) (Supra 35-VP, Carl Zeiss, Germany). Ultraviolet–visible (UV–vis) spectroscopy (Cary 5G equipment) provided optical reflectance spectra of ZnS powders.

PL spectra were collected with a Thermal Jarrel-Ash Monospec monochromator and a Hamamatsu R446 photomultiplier. The 350.7 nm exciting wavelength of a krypton ion laser (Coherent Innova) was used; the output of the laser was maintained at 200 mW. All measurements were taken at room temperature.

An inductively coupled plasma atomic emission spectrometer (ICP-AES) simultaneous CCD–VISTA–MPX (Varian) with a radial configuration was used for the chemical analysis of ca. 0.0200 g samples. The dissolution procedure was conducted using 10 mL of HCl (37 % purity) in closed vessels at room temperature. Analytical blanks were prepared following the same acid digestion procedure, and the final 100 mL sample solutions were diluted with de-ionized water.

Model system and computational method

Several theoretical research works are based on DFT theory for studies in materials science. Periodic DFT calculations have demonstrated that they are able to reproduce with accuracy the electronic structure of solid state systems. In this study, the periodic DFT calculations with the B3LYP hybrid functional [27, 28] were performed using the CRYSTAL06 computer code [29], which has been successfully employed for studies of electronic and structural properties of diverse compounds [30–33]. CRYSTAL is an ab initio (Hartree-Fock and DFT) LCAO program for the treatment of periodic systems. LCAO, in the present case, means that each crystalline orbital is a linear combination of Bloch functions.

The level of accuracy of the calculation of Coulomb and the exchange series is controlled by five parameters. The 8, 8, 8, 8, 14 parameters was chosen for the Coulomb overlap, Coulomb penetration, exchange overlap, first exchange pseudo-overlap, and second exchange pseudo overlap parameters, respectively. The integration in the reciprocal space was performed by sampling the Brillouin zone with an 6x6x6 pack-Monkhorst.

The ZnS zinc-blend (cubic) structure has just one lattice parameter “a” with two atoms per unit cell; with atomic positions: (0,0,0) and (0.25,0.25,0.25) for Zn and S atoms, respectively.

The atomic centers are described by the entire electron basis set 86-411d31G [34] for Zn and 86-311G* for S [35] atoms. For europium atoms, it is convenient to avoid core

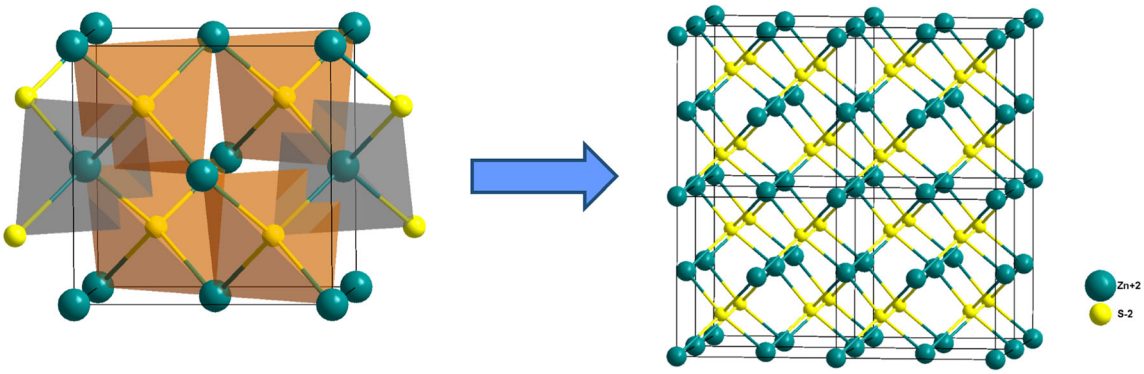

Fig. 1 Pure ZnS 2x2x2 supercell

electrons, and adopt the well-assessed effective core pseudopotential (ECP) techniques [36, 37]. The large-core ECP basis, ECP52MWB [38, 39] (http://www.theochem.uni-stuttgart.de/pseudopotentials) has been chosen to represent the Eu^{3+} in this work. To the best of our knowledge this basis set is the only pseudopotential available and there is no all-electron basis set available to be used in the CRYSTAL program.

A full optimization procedure was carried out to determine the zinc blend equilibrium geometry. The optimized and experimental values (given in parentheses) are a=5.516 (5.40) Å[40].

From this optimized lattice parameter, two 2x2x2 supercell periodic models were used to study the pure and doped ZnS. This supercell contains 32 ZnS units, totaling 64 atoms. The first represents the pure ZnS (p-ZnS) and the second one represents the doped ZnS (d-ZnS) where one Eu atom replaces one Zn atom, resulting in 3.125 % Eu. These models can be useful to represent different behavior and properties in the material.

Figure 1 illustrates a schematic representation for pure ZnS supercell. A new optimization procedure of d-ZnS supercell was made to determine the equilibrium geometry. For these simulations we recommend the use of a symmetric supercell (2x2x2). The new calculated cell parameter is a=5.576 Å, very close to the previous results presented here. The computational cost is dependent on the sueprcell size, large models can be prohibitive.

The band structures were calculated for 100 K points along the appropriate high-symmetry paths of the adequate Brillouin zone. Diagrams of the density of state (DOS) were obtained for analysis of the corresponding electronic structure.

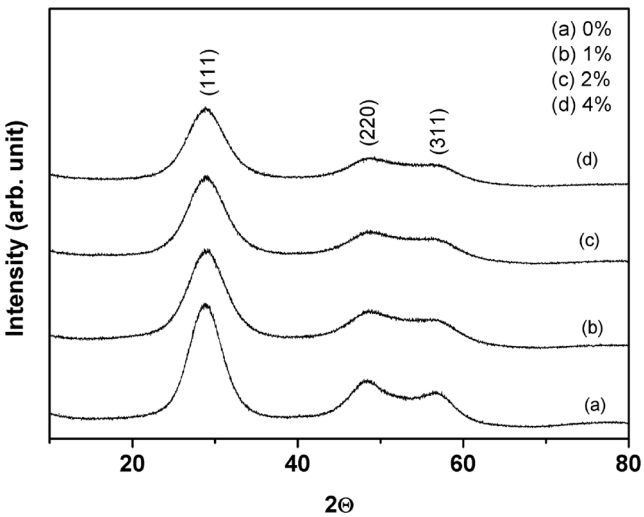

Fig. 2 XRD patterns of ZnS powders with **a**) 0, **b**) 1, **c**) 2, and **d**) 4 % of Eu^{3+} processed in a MAS system at 413 K for 16 min

Results and discussion

Figure 2 illustrates XRD patterns of the samples with three different concentrations of Eu^{3+} in the microwave synthesis which were used to analyze the long-range order. The diffraction peaks indicate a cubic structure which is in agreement with the JCPDS card: 67–790 [40]. Differences observed between the samples indicate structural changes. With the increase of Eu^{3+}, diffraction peaks became broader and less defined which is probably due to ineffective ordering of the lattice. Results of all samples indicate just ZnS diffraction peaks.

Another important aspect concerning the diffraction peaks exposed in Fig. 2 is the significant broadening of the most intense reflections in the XRD patterns which shows the

Table 1 Average of crystallite sizes and ICP-AES results of the ZnS pure and with different Eu^{3+} concentrations

Samples	Crystallite sizes (nm)	ICP-AES	
		Expected	Result
Pure ZnS	3.36	0 %	0 %
ZnS:Eu 1 %	3.01	1 %	1.2 %
ZnS:Eu 2 %	3.00	2 %	2.1 %
ZnS:Eu 4 %	2.94	4 %	2.8 %

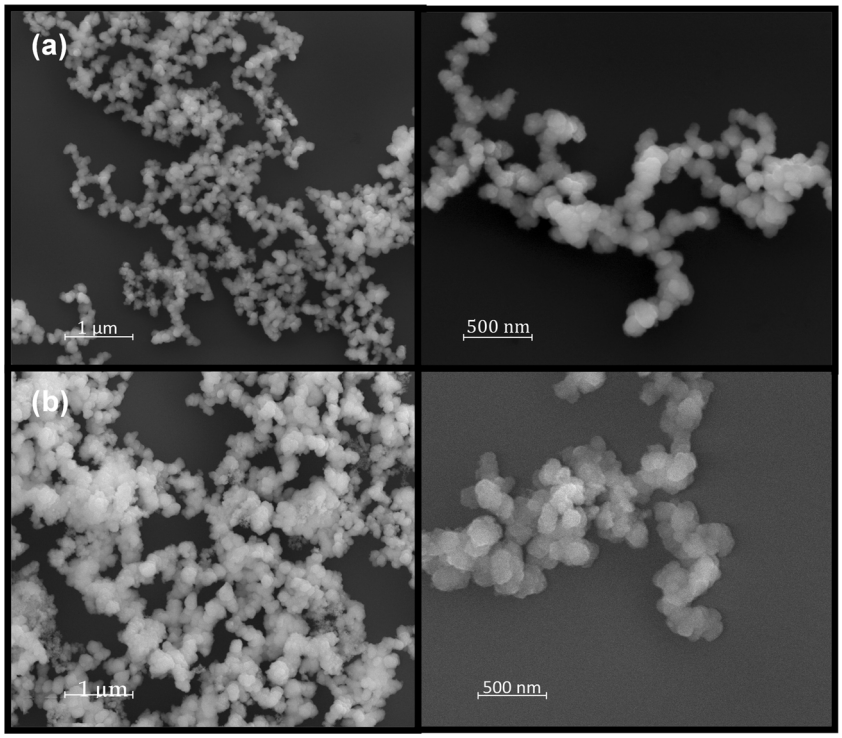

Fig. 3 FE-SEM images of **a**) pure ZnS and **b**) ZnS:Eu 4 %

extent europium is incorporated into the ZnS structure and suggests a decrease in the crystallite size of the material obtained by the MAS method. The average crystallite size of all samples was estimated using the Debye-Scherer method [41]. The equation below encompasses the spherical shape and reduced size of the sample.

Average crystallite size of material $t = k\lambda/\beta \cos\theta$ (01)

where, k is a constant; λ is the wavelength of the x-rays in nm; β is the full width half maximum (FWHM) of the major peak in radians as calculated from XRD peaks data and θ is the diffraction angle.

Estimated size values using the main peak are depicted in Table 1. With the addition of europium, there is an initial decrease in the size, but little variation occurs with the increase of dopant concentration.

To evaluate the dopant arrangement as a substitution ion (or even as a superficial element) a chemical analysis is fundamental. Table 1 shows the expected values of Eu^{3+} calculated according to the amount of precursors added and the results of the ICP-AES technique.

These ICP-AES results indicate that pure ZnS, ZnS:Eu 1 % and ZnS:Eu 2 % are in agreement with the expected

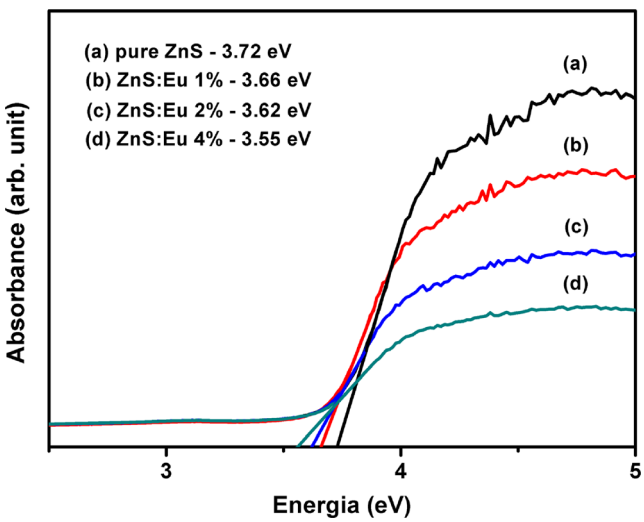

Fig. 4 UV–vis spectra of ZnS powders with **a**) 0 %, **b**) 1 %, **c**) 2 %, and **d**) 4 % of Eu^{3+}

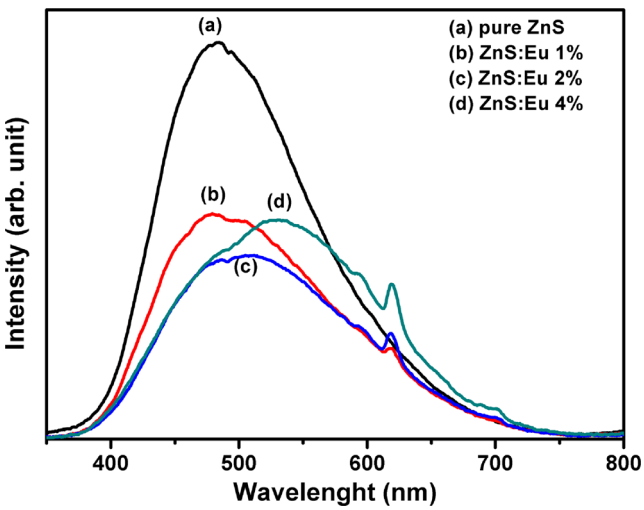

Fig. 5 PL spectrum of ZnS powders at room temperature ($\lambda_{excitation}$ = 350.7 nm); **a**) pure ZnS, **b**) ZnS:Eu 1 %, **c**) ZnS:Eu 2 %, and **d**) ZnS:Eu 4 %

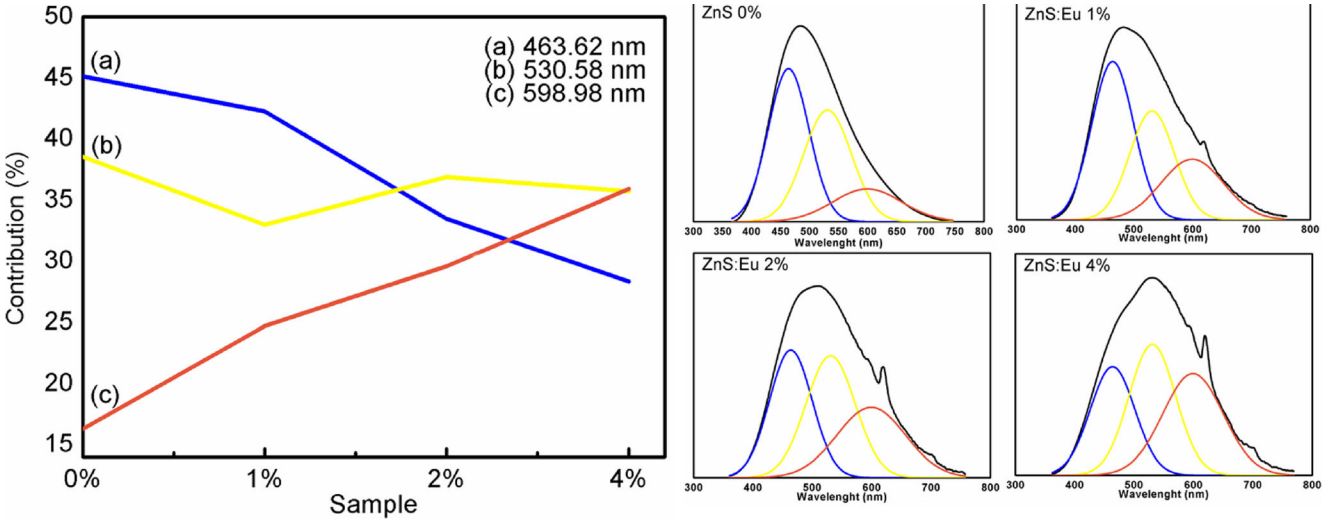

Fig. 6 Deconvoluted PL bands of three curves centered at 463.62 nm, 530.58, nm and 598.98 nm and their contributions

percentage of doping; however, the Zns:Eu 4 % result shows a considerable difference which indicates that Eu^{3+} maximum percentage was achieved in the lattice by this method. The percentage of Eu in relation to Zn is slightly lower than expected mainly due to the ZnS synthesis yield.

Figure 3 shows a FE-SEM image for pure and ZnS:Eu 4 % after 16 min in the microwave. In both cases, the particles are agglomerated, spherical, and of varying sizes. These conditions were not sufficient to avoid the agglomeration and possible particle coalescence. No major differences were observed between the samples.

Gap energy values can be obtained by the Wood and Tauc method [42] using UV–vis spectroscopy (see Fig. 4).

The UV–vis spectra indicate a decrease in behavior of the energy gap as a function of dopant concentration (3.72 eV to 3.55 eV). Clusters formed by the europium replacement, EuS_4, create a different local charge density when compared with ZnS_4 clusters. Furthermore, the different dopant charge can provide the formation regarding vacancies or interstitial defects (due to the different charge density of Eu^{3+} ion) in the ZnS host lattice. These defects introduce a symmetry breakdown and, as a consequence, an introduction of a new energy level in the forbidden region. Several research works show the variation of the semiconductor band gap caused by structure change [43–46].

Figure 5 shows the PL emission spectra of pure and doped ZnS powders recorded at room temperature with excitation at 350.7 nm. The emission spectra show a broad band centered at ~484 nm which may be attributed to ZnS matrix, and the profile of emission band is typical of a multi-phonon and multilevel; i.e., a system in which relaxation occurs by several paths involving the participation of numerous states within the band gap of the semiconductor.

The PL emission spectra of doped ZnS powders show that the maximum emission bands are centered at 498, 510, and 534 nm, for 1 %, 2 %, and 4 % Eu^{3+}, respectively. Therefore, a red shift emission was observed with the increase of europium concentration. The emission spectra show the characteristic narrow band assigned to $^5D_0$-$^7F_2$ transitions in Eu^{3+} at 612 nm

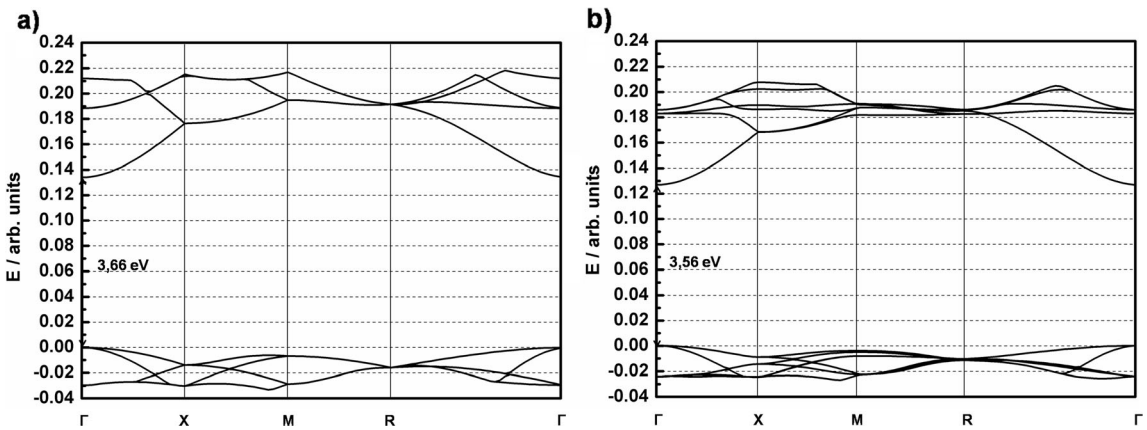

Fig. 7 Band structures of **a**) p-ZnS and **b**) d-ZnS models

in all doped samples. This suggests the incorporation of Eu^{3+} ion in the ZnS nanoparticles did not change its radiative relaxation processes. The red shift effect denotes a strong influence of the europium orange lines emission associated to the allowed transitions originated from electronic reconfiguration.

To obtain a better understanding about the PL modifications in relation to the structural defects caused by the dopant, PL emission spectra were analyzed using decomposition PeakFit. The contribution of each deconvoluted curve and its variations are depicted in Fig. 6. Upon deconvolution, three pseudo-voids were chosen to describe the emissions; i.e., 463.62 nm (blue), 530.58 nm (yellow), and 598.98 nm (orange) labeled as *a*, *b*, and *c*, respectively.

Pure ZnS has a greater contribution from the blue region; however, with the addition of europium and its increase, the contributions from the blue region decrease while the contribution from the orange region increases. The europium, besides its well defined bands, has modified the wide band of the matrix in the region between the orange and the red emissions, which indicates deep defects as a consequence of a different charge density in the lattice due to the Eu addition.

To gain a better understanding of differences caused by the introduction of europium in PL results and the variations

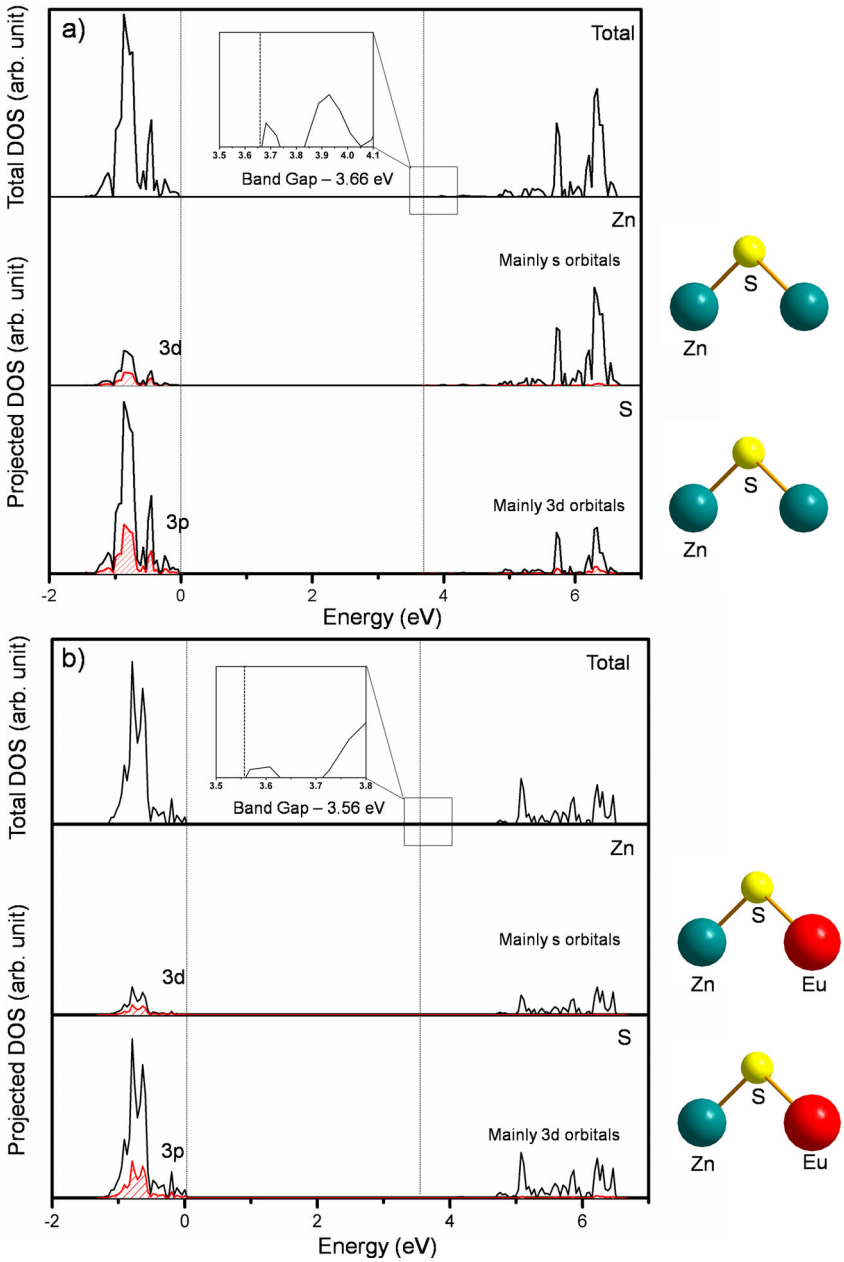

Fig. 8 DOS of **a**) p-ZnS and **b**) d-ZnS models

observed in the atomic orbitals, theoretical models of pure ZnS (p-ZnS) and doped ZnS (d-ZnS) were made. The doped models are not an exact replication of all modifications caused by the dopant in the lattice. The symmetry was maintained in both instances and the system d-ZnS has 3.125 % of europium.

Simulation results of band structure (Fig. 7) indicate a direct band gap at the Γ point in both models. The band gap values of p-ZnS and d-ZnS were 3.66 eV and 3.56 eV, respectively. Although there are limitations in simulating the experimental system, the theoretical and experimental results show the same behavior, i.e., the band gap decreases from pure to doped system.

Figure 8 shows the density of states (DOS) of p-ZnS and d-ZnS models

The DOS is very useful to verify different transition levels locations and band compositions. Comparing the total DOS (see Fig. 8a and b), the addition of 3.125 % of Eu^{3+} in the lattice generated a considerable modification of the profile.

An analysis of the projected DOS in both cases (p-ZnS and d-ZnS) for Zn atoms, indicates that the valence band (VB) consists mainly of 3d ($3d_{x-y}$, $3d_{x-z}$, $3d_{y-z}$, $3d_{x^2-y^2}$, and $3d_{z^2}$) levels with a minor contribution of 3p ($3p_x$, $3p_y$, and $3p_z$). The ionic characteristic of the ZnS causes the oxidation state of Zn to remain near to 2+. The conduction band (CB) of the Zn (greatest contribution of the CB of the total DOS) comes mainly from the "s" orbitals. The DOS of the S atoms show that VB is composed mainly from $3p_x$, $3p_y$, and $3p_z$ orbitals while the CB is derived mainly from "d" levels. Quantum-mechanical calculations for d-ZnS indicate that localized states generated in the band gap reduce the gap energies. These findings corroborate with the experimental evidence of the incorporation of Eu^{3+} in the lattice. The characteristic energy structure of the nanoparticles can explain why the energy transfer from nanosized ZnS host to Eu^{3+} ions is so efficient. This mixing transforms the forbidden transitions of Eu^{3+} ions to allowed transitions, which results in broadening of the transition peaks of Eu^{3+} activators in ZnS nanoparticles. Another benefit of the mixing is an enhanced energy transfer rate to the *d-f* electronic levels of Eu^{3+}.

A correlation can be made between the involved orbitais and PL results. According to the wide band model [47, 48] there are three necessary steps: excitation, recombination, and emission. The first step consists basically of the absorption of energy, corresponding mainly to the transition from "S 3p" orbitals states at the valence up to "Zn 4s" orbitals states inside the forbidden band gap. After excitation, there are recombination processes that occur among the excited states closer to the CB. Finally, there is emission due to the return of the electron to the ground state.

To verify the polarization created by the introduction of dopant in the system, Fig. 9 shows a charge density map of a sulfur layer near to the position where the europium was added:

As a reminder, the computational model considers the pure system as a perfect crystal, with no defects. According to the simulation, all Zn atoms have the same charge and all S atoms have the opposite charge, and thus there is no polarization. For this reason the sulfur layer (see Fig. 8a) has the same pattern. However, the equality of the charge is modified when europium is present in the structure. The introduction of the impurity in the lattice changes the charges of Zn and S atoms as an approximation for the europium atom. Figure 8b shows that there is a visual modification in the sulfur layer in the europium region only; i.e., this impurity generates a polarization in the lattice which is responsible for modifications in the DOS. This structure generates greater local imbalanced charges and the formation of static electrons and holes in the lattice. Noticeably, the polarizations around this new cluster coordination change the structural configurations around europium atoms.

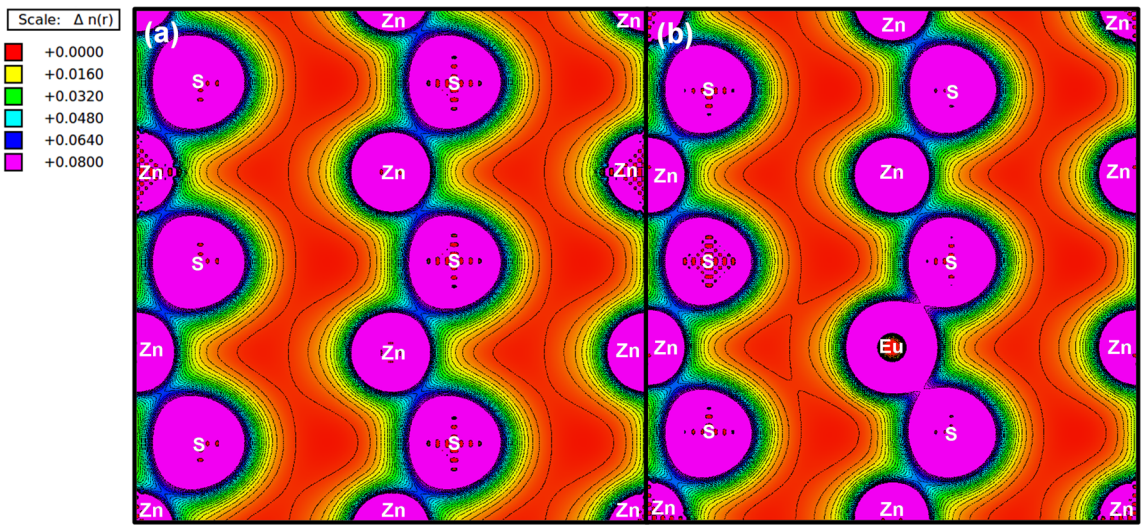

Fig. 9 Electron density maps of **a**) p-ZnS and **b**) d-ZnS models

New localized states generated by the addition of Eu^{3+} in the forbidden band gap region increase the probability of fewer energy transitions which causes a red shift in the PL bands.

Conclusions

In summary, the MAH method has shown itself very efficient and facile to the synthesis of ZnS and ZnS:Eu. Structural analyses were conducted through XRD and FE-SEM. To complement experimental results, a quantum-chemical modeling was made based on the DFT and periodic supercell models in order to evaluate the symmetry of the system. The chemical analysis (ICP-AES) indicated a Eu^{3+} saturation in percentages up to 2.8 %.

In this work, experimental results showed that the addition of Eu^{3+} in the cubic ZnS lattice causes disorder in the structure and the modification of the optical properties.

To complement the studies of the change modifications by the dopant, theoretical studies showed the addition of Eu^{3+} in Zn position causes a symmetry breaking and a local polarization in the structure. The difference of the simulated band gap between pure and doped models showed a great similarity with experimental results. Besides that, by means of DOS it was possible to verify the modification of the profile of the electronic levels.

Therefore the red shift in the PL profile according to the dopant amount can be attributed to new intermediate levels in the band gap region, which are generated by structure defects as distortions or vacancies as was confirmed by first-principles calculations.

Acknowledgments The authors appreciate the support of the Brazilian research financing institutions: CAPES, FAPESP (2012/14468-1, 2012/22823-6 2012/07967-1, 2013/07296-2, 2013/19289-0), and CNPq (573636/2008-7).

References

1. Zhang C, Lin J (2012) Defect-related luminescent materials: synthesis, emission properties and applications. Chem Soc Rev 41:7938–7961
2. Liu Y, Tu D, Zhu H, Li R, Luo W, Chen X (2010) A Strategy to achieve efficient dual-mode luminescence of Eu^{3+} in lanthanides doped multifunctional $NaGdF_4$ nanocrystals. Adv Mater 22:3266–3271
3. Blasse G, Grabmaier BC (1994) Luminescence mater. Springer, Berlin
4. Reisfeld RJ, Christian KJ (1977) Lasers and excited states of rare earths. Ber Bunsen Phys Chemie 82:844–844
5. Zhang K, Yu Y, Sun S (2012) Influence of Eu doping on the microstructure and photoluminescence of CdS nanocrystals. Appl Surf Sci 258:7658–7663
6. Sadhu S, Chowdhury PS, Patra A (2007) Understanding the role of particle size on photophysical properties of CdS:Eu^{3+} nanocrystals. J Lumin 126:387–392
7. Wen X, Li M, Wang Y, Zhang J, Fu L, Hao R, Ma Y, Ai X (2008) Colloidal nanoparticles of a europium complex with enhanced luminescent properties. Langmuir 24:6932–6936
8. Silva D, Abreu A, Davolos MR, Rosaly M (2011) Determination of the local site occupancy of Eu^{3+} ions in $ZnAl_2O_4$ nanocrystalline powders. Opt Mater 33:1226–1233
9. Ekambaram S (2005) Effect of host-structure on the charge of europium ion. J Alloy Compd 390:L1–L3
10. Sapra S, Prakash A, Ghangrekar A, Periasamy N, Sarma DD (2005) Emission properties of manganese-doped ZnS nanocrystals. J Phys Chem B 109:1663–1668
11. Biswas S, Kar S (2008) Fabrication of ZnS nanoparticles and nanorods with cubic and hexagonal crystal structures: a simple solvothermal approach. Nanotechnology 19
12. Tran TK, Park W, Tong W, Kyi MM, Wagner BK, Summers CJ (1997) Photoluminescence properties of ZnS epilayers. J Appl Phys 81:2803–2809
13. Ong HC, Chang RPH (2001) Optical constants of wurtzite ZnS thin films determined by spectroscopic ellipsometry. App Phys Lett 79: 3612–3614
14. Peng WQ, Qu SC, Cong GW, Wang ZG (2005) Concentration effect of Mn2+ on the photoluminescence of ZnS : Mn nanocrystals. J Cryst Growth 279:454–460
15. Lee SY, Shin YH, Kim Y, Kim S, Ju S (2011) Thermal quenching behavior of emission bands in Eu-doped ZnS nanowires. J Luminescence 131:1336–1339
16. Wang L, Xu X, Yuan X (2010) Preparation and photoluminescent properties of doped nanoparticles of ZnS by solid-state reaction. J Luminescence 130:137–140
17. Ashwini K, Pandurangappa C, Nagabhushana BM (2012) Synthesis and optical properties of undoped and Eu-doped ZnS nanoparticles. Phys Scripta 85:065706
18. Amaranatha Reddy D, Murali G, Poornaprakash B, Vijayalakshmi RP, Reddy BK (2012) Effect of annea ling temperature on optical and magnetic properties of Cr doped ZnS nanoparticles. Solid State Commun 152:596–602
19. Planelles-Arago J, Julian-Lopez B, Cordoncillo E, Escribano P, Pelle F, Viana B, Sanchez C (2008) Lanthanide doped ZnS quantum dots dispersed in silica glasses: an easy one pot sol–gel synthesis for obtaining novel photonic materials. J Mater Chem 18:5193–5199
20. Thostenson ET, Chou TW (1999) Microwave processing: fundamentals and applications. Compos Part A Appl S 30:1055–1071
21. Komarneni S, Roy R, Li QH (1992) Microwave-hydrothermal synthesis of ceramic powders. Mater Res Bull 27:1393–1405
22. Cavalcante LS, Longo VM, Sczancoski JC, Almeida MAP, Batista AA, Varela JA, Orlandi MO, Longo E, Li MS (2012) Electronic structure, growth mechanism and photoluminescence of $CaWO_4$ crystals. Cryst Eng Comm 14:853–868
23. Raubach CW, de Santana YVB, Ferrer MM, Longo VM, Varela JA, Avansi W Jr, Buzolin PGC, Sambrano JR, Longo E (2012) Strutural and optical approach of CdS@ZnS core–shell system. Chem Phys Lett 536:96–99
24. de Santana YVB, Raubach CW, Ferrer MM, La Porta F, Sambrano JR, Longo VM, Leite ER, Longo E (2011) Experimental and theoretical studies on the enhanced photoluminescence activity of zinc sulfide with a capping agent. J Appl Phys 110:123507–123507
25. Ferrer MM, de Santana YVB, Raubach CW, Sambrano JR, Longo E (2013) Experimental and theoretical studies of photoluminescence in ZnS obtained by microwave-assisted solvothermal method. Curr Phys Chem 3:413–418
26. La Porta FA, Ferrer MM, de Santana YVB, Raubach CW, Longo VM, Sambrano JR, Longo E, Andrés J, Li MS, Varela JA (2013)

Synthesis of wurtzite ZnS nanoparticles using the microwave assisted solvothermal method. J Alloy Compd 556:153–159
27. Becke AD (1993) Density-functional thermochemistry.3. the role of exact exchange. J Chem Phys 98:5648–5652
28. Lee C, Yang W, Parr RG (1988) Development of the colle-salvetti correlation-energy formula into a functional of the electron density. Phys Rev B 37:785–789
29. Dovesi RS, Saunders VR, Roetti C, Orlando R, Zicovich-Wilson CM, Pascale F, Civalleri B, Doll K, Harrison NM, Bush IJ, D'Arco P, Llunell M (2009) Crystal09 user's manual. University of Torino, Torino
30. Marana NL, Longo VM, Longo E, Martins JBL, Sambrano JR (2008) Electronic and structural properties of the (10(1)over-bar0) and (11(2)over-bar0) ZnO surfaces. J Phys Chem A 112:8958–8963
31. Moreira ML, Buzolin PGC, Longo VM, Nicoleti NH, Sambrano JR, Li MS, Varela JA, longo e joint experimental and theoretical analysis of order disorder effects in cubic BaZrO(3) assembled nanoparticles under decaoctahedral shape. J. Phys. Chem. A 115:4482–4490
32. Sambrano JR, Longo VM, Longo E, Taft CA (2007) Electronic and structural properties of the (001) $SrZrO_3$ surface. J Mol Struct (THEOCHEM) 813:49–56
33. Sambrano JR, Nóbrega GF, Taft CA, Andrés J, Beltrán A (2005) A theoretical analysis of the TiO_2/Sn doped (1 1 0) surface properties. Surf Sci 580:71–79
34. Jaffe JE, Hess AC (1993) Hartree-fock study of phase changes in ZnO at high pressure. Phys Rev B 48:7903–7909
35. Lichanot A, Aprà E, Dovesi R (1993) Quantum Mechnical Hartree-Fock Study of the Elastic Properties of Li_2S and Na_2S. Phys Status Solidi B 177:157–163
36. Hay PJ, Wadt WR (1985) Ab initio effective core potentials for molecular calculations potentials for the transition metal atoms Sc to Hg. J Chem Phys 82:270–283
37. Durand P, Barthelat JC (1975) A theoretical method to determine atomic pseudopotentials for electronic structure calculations of molecules and solids. Theoret Chim Acta 38:283–302
38. Eick HA, Baenziger NC, Eyring L (1956) The preparation, crystal structure and some properties of SmN, EuN and YbN1. J Am Chem Soc 78:5987–5989
39. Eick HA, Baenziger NC, Eyring L (1956) Lower oxides of samarium and europium. the preparation and crystal structure of $SmO_{0.4–0.6}$, SmO and EuO_1. J Am Chem Soc 78:5147–5149
40. Yeh CY, Lu ZW, Froyen S, Zunger A (1992) Zinc-blende-wurtzite polytypism in semiconductors. Phys Rev B 46:10086–10097
41. Klug HP, Alexander LA (1962) X-ray diffraction procedures. Wiley, New York
42. Wood DL, Tauc J (1972) Weak absorption tails in amorphous semiconductors, Phys. Rev. B 5:3144-&
43. Cavalcante LS, Sczancoski JC, Li MS, Longo E, Varela JA (2012) β-ZnMoO4 microcrystals synthesized by the surfactant-assisted hydrothermal method: growth process and photoluminescence properties. Coll Surf A: Phys Eng Asp 396:346–351
44. Cavalcante LS, Almeida MAP, Avansi W, Tranquilin RL, Longo E, Batista NC, Mastelaro VR, Li MS (2012) Cluster coordination and photoluminescence properties of α-Ag_2WO_4 microcrystals. Inorg Chem 51:10675–10687
45. Moreira ML, Longo VM, Avansi W, Ferrer MM, Andrés J, Mastelaro VR, Varela JA, Longo E (2012) Quantum mechanics insight into the microwave nucleation of SrTiO3 nanospheres. J Phys Chem C 116: 24792–24808
46. Willardson RK, Goering HL (1962) Compound semiconductors. Reinhold, New York
47. Longo VM, Cavalcante LS, de Figueiredo AT, Santos LPS, Longo E, Varela JA, Sambrano JR, Paskocimas CA, De Vicente FS, Hernandes AC (2007) Highly intense violet-blue light emission at room temperature in structurally disordered SrZrO(3) powders. Appl Phys Lett 90
48. Moreira ML, Paris EC, do Nascimento GS, Longo VM, Sambrano JR, Mastelaro VR, Bernardi MIB, Andres J, Varela JA, Longo E (2009) Structural and optical properties of CaTiO(3) perovskite-based materials obtained by microwave-assisted hydrothermal synthesis: an experimental and theoretical insight. Acta Mater 57:5174–5185